Peridinin Chlorophyll *a* Protein: Relating Structure and Steady-State Spectroscopy†

Foske J. Kleima,‡ Markus Wendling,‡ Eckhard Hofmann,§ Erwin J. G. Peterman,‡ Rienk van Grondelle,‡ and Herbert van Amerongen*,‡

Faculty of Sciences, Division of Physics and Astronomy, and Institute for Condensed Matter Physics and Spectroscopy, Vrije Universiteit Amsterdam, De Boelelaan 1081, 1081 HV Amsterdam, The Netherlands, and Fakultät für Biologie, Universität Konstanz, Box M656, D-78457 Konstanz, Germany

Received October 19, 1999; Revised Manuscript Received January 20, 2000

ABSTRACT: Peridinin chlorophyll *a* protein (PCP) from *Amphidinium carterae* has been studied using absorbance (OD), linear dichroism (LD), circular dichroism (CD), fluorescence emission, fluorescence anisotropy, fluorescence line narrowing (FLN), and triplet-minus-singlet spectroscopy (T-S) at different temperatures (4−293 K). Monomeric PCP binds eight peridinins and two Chls *a*. The trimeric structure of PCP, resolved at 2 Å [Hofmann et al. (1996) *Science 27*, 1788−1791], allows modeling of the Chl *a*−protein and Chl *a*−Chl *a* interactions. The FLN spectrum shows that Chl *a* is not or is very weakly hydrogen-bonded and that the central magnesium of the emitting Chl *a* is monoligated. Simulation of the temperature dependence of the absorption spectra indicates that the Huang−Rhys factor, characterizing the electron−phonon coupling strength, has a value of ∼1. The width of the inhomogeneous distribution function is estimated to be 160 cm^{-1}. LD experiments show that the two Chls *a* in PCP are essentially isoenergetic at room temperature and that a substantial amount of PCP is in a trimeric form. From a comparison of the measured and simulated CD, it is concluded that the interaction energy between the two Chls *a* within one monomer is very weak, <10 cm^{-1}. In contrast, the Chls *a* appear to be strongly coupled to the peridinins. The 65 cm^{-1} band that is visible in the low-frequency region of the FLN spectrum might indicate a Chl *a*−peridinin vibrational mode. The efficiency of Chl *a* to peridinin triplet excitation energy transfer is ∼100%. On the basis of T-S, CD, LD, and OD spectra, a tentative assignment of the peridinin absorption bands has been made.

The overall efficiency of photosynthesis is strongly enhanced by the light-harvesting complexes that transfer absorbed light energy to the reaction centers (*1*). Photosynthetic dinoflagellates, forming the major component of sea plankton, contain several membrane-bound light-harvesting complexes similar to those in higher plants and green algae. These organisms contain also water-soluble light-harvesting complexes, peridinin chlorophyll *a* proteins (PCP).[1] The predominant carotenoid of dinoflagellates is peridinin, which enables the organism to collect light in the 470−550 nm region where chlorophyll does not absorb. The structure of PCP from the dinoflagellate *Amphidinium carterae* has been resolved by X-ray crystallography to a resolution of 2.0 Å (*2*).

Monomeric PCP from *A. carterae* contains two chlorophylls *a* (Chl *a*) and eight peridinins. These pigments are organized in two clusters, each containing one Chl *a* and four peridinins. Each peridinin molecule is in van der Waals contact with the tetrapyrrole ring of the Chl *a* of the same cluster. The center-to-center distance between the two Chls *a* is 17.4 Å (*2*). The peridinin molecules are organized in two pairs per cluster, where the closest distance between the polyene chains within a pair is less than 4 Å (*2*). The pigment clusters are located in the hydrophobic cavity formed by the protein. The peptide primary sequences of the NH_2 and COOH terminal regions are largely (56%) homologous and form structurally almost identical domains each consisting of eight α-helices (*2*). The holoprotein, including also two lipid molecules, has a molecular weight of 38.1 kDa. In the crystals, the complex is trimeric.

Long before the structure of PCP was resolved, the complex was isolated and studied spectroscopically (*3*, *4*). The peridinin to chlorophyll *a* excitation energy transfer was shown to have an efficiency of 88% (*5*)−100% (*3*) and to occur on a time scale of a few picoseconds (*5*). The circular dichroism (CD) spectrum has been interpreted in terms of exciton interactions between peridinins (*6*). Triplet-minus-singlet (T-S) experiments show efficient transfer of triplet excitation energy from Chl *a* to peridinin (*5*). These studies were mainly focusing on peridinin−peridinin and peridinin−Chl *a* interactions.

† H.v.A. and R.v.G. were supported by the Dutch science foundation (FOM). M.W. received a Marie Curie Fellowship (EC Grant ERB FMBICT 960842).

* Corresponding author telephone: +31-20-4447932; fax: +31-20-4447999; e-mail: herbert@nat.vu.nl

‡ Vrije Universiteit Amsterdam.

§ Universität Konstanz.

[1] Abbreviations: CD, circular dichroism; Chl *a*, Chlorophyll *a*; Chls, chlorophylls; Cytb_6f, cytochrome b_6f complex; DADS, decay associated difference spectra; ϕ_n, orientation factor; FLN, fluorescence line narrowing; IDF, inhomogeneous distribution function; LD, linear dichroism; LD_r, reduced linear dichroism; LHCII, light-harvesting complex II of green plants; μ^2, dipole strength; μ^2_{eff}, effective dipole strength; *n*, refractive index; OD, optical density; PCP, peridinin Chl *a* protein; PSIIRC, photosystem II reaction center; PW, phonon wing; RT, room temperature; S, Huang−Rhys factor; T-S, triplet-minus-singlet spectroscopy; V, exciton interaction energy; v/v, volume per volume; w/v, weight per volume; ZPL, zero phonon line; ζ, angle between the transition dipole moment and the symmetry axis.

10.1021/bi992427s CCC: $19.00
Published on Web 04/06/2000

PCP forms an ideal system to study Chl *a*−protein and Chl *a*−Chl *a* interactions for the following reasons: (i) a limited number of Chls *a* are bound, (ii) a high-resolution crystal structure is available, and (iii) the peridinins do not contribute to the absorption in the Chl *a* Q_y region, so that in this region the absorption is entirely due to a few Chl *a* molecules. Here, we present a study that to a large extent deals with the properties of Chl *a* in PCP. Information about the electron−phonon coupling and the vibrational modes of Chl *a* in PCP is obtained from fluorescence line narrowing (FLN) experiments. Furthermore, the 580−630 nm region of the absorption spectrum of PCP is interpreted in detail. The linear dichroism (LD) spectrum provides information about the site energies of the Chls *a* in PCP. In addition, a simulation of the CD spectrum in the Chl *a* Q_y region is presented. On the basis of a combination of the spectral features revealed by T-S, absorption, LD, and CD spectra in the peridinin region, a tentative assignment of the absorption bands of peridinin in PCP is obtained.

MATERIALS AND METHODS

Sample Preparation and Spectroscopy. PCP from *A. carterae* was prepared as described in ref *2*. The 77 and 4 K measurements were performed in a buffer containing 25 mM Tris (pH 7.5), 3 mM NaN_3, 2 mM KCl, and 85% (v/v) glycerol. For the LD measurements, a gelatin gel was prepared, since the use of a polyacrylamide gel led to the immediate loss of the characteristic orange color of PCP. To a buffer containing 66% (v/v) glycerol, 25 mM Tris (pH 7.5), 3 mM NaN_3, 2 mM KCl, and 6.4% (w/v) gelatin (Dr Oetker) were added, and the mixture (with a volume of 3 mL) was heated to 65 °C in a water bath to dissolve the gelatin. Subsequently, the mixture was cooled to 30 °C, and PCP was added (∼20 μL). Then the mixture was poured into the gel press and kept in the refrigerator for 1 h. After that time, the gel was squeezed by a factor of 1.1 in the *x* and *y* directions, allowing expansion in the *z* direction. The rest of the procedure was described before (*7*). This process led to a PCP gel with an absorption spectrum identical to that of the original sample.

Absorption spectra were measured on a Cary 219 spectrophotometer with a bandwidth of 0.5 nm. CD and LD measurements (bandwidth of 1 nm) were performed on a home-built setup as described earlier (*7*).

Fluorescence spectra were recorded as described previously with a CCD camera (Chromex Chromcam) via a 1/2-m spectrograph (Chromex 500IS) (*8*). Excitation light was provided by a tungsten−halogen lamp via an interference band-pass filter (610 nm, fwhm of 15 nm) or by a dye laser (Coherent CR599, dye DCM, spectral bandwidth 1 cm^{-1}) pumped by an Ar^+ laser (Coherent Innova 310). An optical density (OD) of 0.1 at 670 nm was used for the fluorescence measurements unless stated differently. The measuring time per excitation wavelength was 1 min. The effects of spectral holeburning were minimized by the use of a low laser power (<200 $\mu W/cm^2$), although even at these intensities a decrease (<10%) of the fluorescence intensity was observed. Emission spectra were corrected for the wavelength-dependent sensitivity of the detection system, and the wavelength calibration was checked with an argon calibration lamp.

Microsecond laser-flash induced T-S absorption difference measurements were performed as reported earlier (*9*). In short, excitation pulses at 590 nm were provided by a Nd:YAG (second harmonic) pumped dye laser (Rhodamine 610) and had an intensity of ∼10 mJ. A pulsed xenon lamp was used for detection. The light was detected via a 1/4-m monochromator (bandwidth 2 nm) by a photomultiplier connected to a digital oscilloscope. The response time of the setup was less than 0.5 μs. Time traces (averages of 32 shots) were detected at different detection wavelengths and analyzed globally (*10*). At 590 nm, mainly Chl *a* is excited, but the excitation of some peridinin cannot be ruled out.

Calculation of LD. If the orientations of the transition dipole moments of pigments in a pigment−protein complex and the orientation behavior of the complexes in a (compressed) gel are known, the reduced LD (LD_r) can be calculated using the following expression (*11*):

$$LD_r = \frac{\Delta A}{3A} = \langle 0.5(3\cos^2\zeta - 1)\rangle \phi_n \qquad (1)$$

where ΔA is the measured LD spectrum, A is the isotropic absorption spectrum, and ζ is the angle between the transition dipole moment and the molecular axis of the complex (see below). The brackets $\langle\ \rangle$ denote averaging over different pigments within a single complex. ϕ_n is an orientation factor that reflects how (well) the complexes are oriented on average. This factor is negative for disklike particles and positive for rodlike particles. The molecular axis for disklike particles is the axis perpendicular to the plane of the disk, whereas for rodlike particles, the longest axis is defined as the molecular axis (*11*).

Monte Carlo Simulation of OD and CD Spectra. To interpret the height of the CD spectrum, we have performed a Monte Carlo simulation to calculate the OD and CD spectra at room temperature. A more detailed analysis of the absorption spectrum at various temperatures is given in the Discussion section where the contributions from homogeneous and inhomogeneous broadening are estimated. The Monte Carlo method is essentially the same as described in ref *12*. In short, for each run, an interaction matrix was generated with the site energies on the diagonal and the interaction energies on the off-diagonal positions. The site energies were picked at random from a Gaussian distribution (see below) to account for the broadening of the spectra. The interaction energies were calculated from the crystal structure. In the case of PCP, the interacting pigments are not charged, and the distances between the pigments are significantly larger than the conjugated parts of the molecules so that the dipole−dipole approximation can be applied (*13*). For Chl *a* in ethanol/methanol, a dipole strength (μ^2) of 28.3 D^2 can be calculated from the absorption spectra in methanol and ethanol when the effect of the medium is ignored. Taking into account the effect of the medium by applying the cavity-field expression for the local field correction factor (*14*), a value of 27.5 D^2 is obtained. The exciton interaction energy V (in cm^{-1}) between two identical pigments can be calculated using (see, for example, refs *15* and *16*):

$$V_{12} = \frac{f_l^2 \mu^2}{\epsilon_r} \frac{5.04\kappa}{R^3} = \mu_{\text{eff}}^2 \frac{5.04\kappa}{R^3} \qquad (2)$$

where R is the distance between the centers of the pigments (in nm), ϵ_r is the relative dielectric constant, and f_l is the

local field correction factor. It was concluded in ref *17* on the basis of Förster calculations that the refractive index of PCP is 1.6 ± 0.1. The effective dipole strength of Chl *a* in PCP can thus be calculated to be 17.0 ± 1.4 D^2, using again the cavity-field expression.

The expression for the orientation factor κ is

$$\kappa = \hat{\mu}_1\hat{\mu}_2 - 3(\hat{\mu}_1\hat{r}_{12})(\hat{\mu}_2\hat{r}_{12}) \quad (3)$$

where $\hat{\mu}_1$ and $\hat{\mu}_2$ are the normalized transition dipole moment vectors, and $\hat{r}_{12}$ is the normalized vector between the centers of pigments 1 and 2.

Using an effective dipole strength of 17.0 D^2 and taking the Q_y transition dipole moment along the *y* axis lead to the following interaction matrix for the full trimer:

$$\begin{bmatrix} \epsilon_1 & -7.1 & 0.7 & -1.2 & 0.7 & -0.3 \\ -7.1 & \epsilon_2 & -0.3 & 0.7 & -1.2 & 0.7 \\ 0.7 & -0.3 & \epsilon_3 & -7.1 & 0.7 & -1.2 \\ -1.2 & 0.7 & -7.1 & \epsilon_4 & -0.3 & 0.7 \\ 0.7 & -1.2 & 0.7 & -0.3 & \epsilon_5 & -7.1 \\ -0.3 & 0.7 & -1.2 & 0.7 & -7.1 & \epsilon_6 \end{bmatrix}$$

In the case of a monomer, it suffices to diagonalize a 2 × 2 matrix (for instance, the upper left part). Interactions with the carotenoids are not included. The site energies (the diagonal entries ϵ_1 ..... ϵ_6) were selected randomly from a Gaussian distribution with a fwhm of 280 cm^{-1} to produce the correct absorption bandwidth. The average site energy was 14 925 cm^{-1}. This matrix was diagonalized numerically, and the eigenvectors and eigenvalues were used to calculate stick spectra. Typically, 100 000 runs were performed. It should be noted that both homogeneous and inhomogeneous broadening contribute to the absorption band shape, but lumping both into one inhomogeneous distribution of site energies is a very good approximation, especially since the interaction strength is much weaker than the bandwidth (*18*).

The CD spectrum is determined by the rotational strengths of the absorption bands of the pigment−protein complex according to ref *18*:

$$\frac{\mathrm{CD}}{\mathrm{OD}} = \frac{A_\mathrm{L} - A_\mathrm{R}}{A} = \frac{4R_j}{D_j} \quad (4)$$

with

$$R_j = \frac{D_j^\mathrm{L} - D_j^\mathrm{R}}{4} = -\frac{\pi n}{2\lambda_{k,m=1}} \sum^{N} C_{jk}C_{jm}(\boldsymbol{r}_{km} \cdot \boldsymbol{\mu}_k \times \boldsymbol{\mu}_m) \quad (5)$$

where $A_\mathrm{L} - A_\mathrm{R}$ is the difference in absorption of left and right circularly polarized light, A is the absorption of isotropic light, R_j is the rotational strength, and D_j is the integrated dipole strength. In eq 5, D_j^L and D_j^R are the dipole strengths for left and right circularly polarized light, λ is the wavelength (in a vacuum) corresponding to transition j, $\boldsymbol{r}_{km}$ is the distance between the interacting pigments, n is the refractive index, N is the number of interacting pigments, C_{jk} and C_{jm} are matrix elements of the diagonalized interaction matrix, and $\boldsymbol{\mu}_k$ and $\boldsymbol{\mu}_m$ are the transition dipoles of pigments k and m. Note that the refractive index has been included to correct for the effect of the medium on the wavelength. In principle, one also needs to take into account the shielding effect of the medium on the polarized absorption (change in size of effective transition dipole moment), but this effect is the same for CD and OD. Because we only consider the CD after normalization to the OD, this effect can be ignored. The effect of the medium on the coupling between the pigments is taken into account when the exciton states are calculated and the latter are described by the matrix elements C_{jk} and C_{jm}.

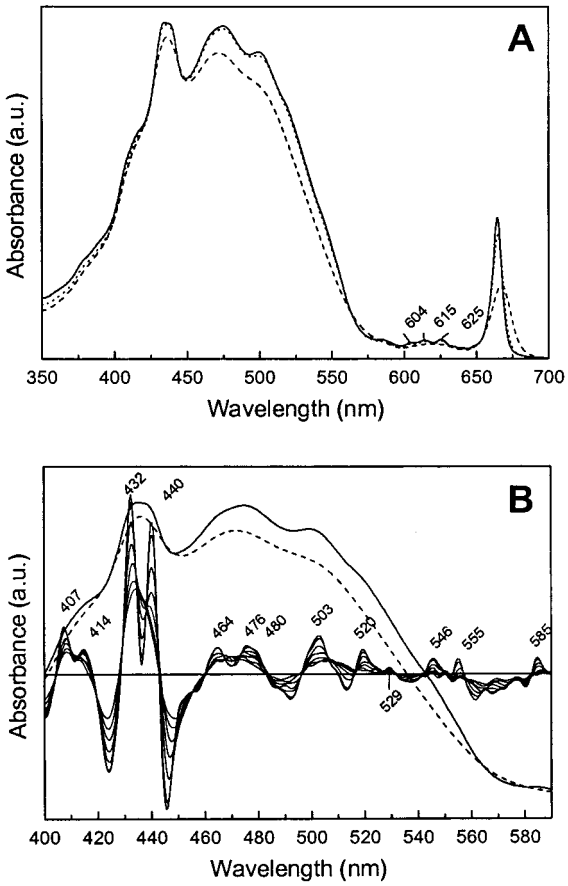

FIGURE 1: (A) OD spectra of PCP at 4 K (solid), 77 K (dotted), and room temperature (RT) (dashed). The peak position of the Chl *a* Q_y band is 665 nm (4 K) and 667.5 nm (RT). (B) Magnification of the 400−590 nm region, showing the RT (dashed) and 4 K (solid) spectrum. Also plotted is the temperature dependence (4 K to RT in steps of 50 K) of the second derivative, which is reversed in sign and rescaled to give a clear picture. Positions of the maxima in the second derivative of the 4 K spectrum (after sign reversal) are indicated in the figure.

Both the simulated CD and the OD spectra are expressed in debye^2 (D^2). For each simulation, the OD spectrum was scaled to the experimental OD spectrum, and the CD spectrum was scaled using the same scaling factor.

RESULTS

Absorption. Absorption spectra measured at 4 K, 77 K, and room temperature (RT) are shown in Figure 1A. The 4 K spectrum shows more structure than the RT spectrum. In the region 600−650 nm, several small peaks appear at 604, 615, and 625 nm. Upon cooling, the peak in the Q_y region at 667.5 nm (RT) shifts almost linearly with temperature to 665 nm at 4 K and sharpens by a factor of ∼2. The apparent overall increase (∼8%) of the absorption upon cooling from RT to 4 K is most likely caused by shrinking of the sample. In the Discussion section, the temperature dependence of the

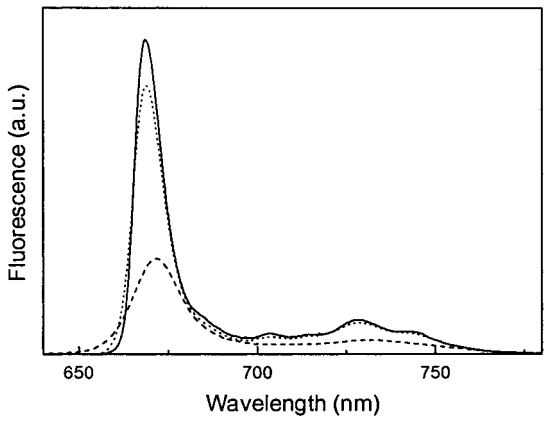

FIGURE 2: Fluorescence emission spectrum of PCP at 4 K (solid), 77 K (dotted), and RT (dashed). The excitation wavelength was 610 nm. At 4 K, the fluorescence peaks at 668.5 nm, and at RT it peaks at 671.5 nm.

second moment of the Q_y band is used to estimate the inhomogeneous line width and the Huang−Rhys factor.

In Figure 1B, the 400−590 nm region of the 4 K and RT spectrum and the second derivatives of the absorption spectra multiplied by −1 as a function of temperature (steps of 50 K) are shown. In the region where peridinin absorbs, the second derivative of the spectrum at 4 K peaks at 464, 476, 480, 503, 520, 529, 546, and 555 nm. These peaks are, albeit at slightly different positions, also present in the second derivatives of spectra measured at higher temperatures (see Figure 1B). The absorption below 440 nm is to a significant extent due to Chl *a*. The peak at 585 nm is most probably due to Chl *a* (*19*, *20*).

Nonselective Fluorescence Spectroscopy. In Figure 2 the fluorescence emission spectra at 4 K, 77 K, and RT after excitation at 610 nm are shown. The integrated intensity of the emission, which is proportional to the fluorescence quantum yield, increases by a factor of 2 upon cooling from RT to 4 K. A similar increase of the quantum yield was reported for the monomeric Chl *a* present in the cytochrome b_6 *f* complex (Cytb_6 *f*) of the cyanobacterium *Synechocystis PCC6803* (*21*). The peak of the fluorescence is located at 668.5 nm (4 K) and shifts to 671.5 nm at RT. The shift is comparable to the peak shift of 2.5 nm of the Q_y band in the OD spectrum (665 to 667.5 nm). The fwhm of the fluorescence spectrum is larger at all temperatures than the fwhm of the absorption spectrum, which was also reported for Cytb_6 *f* (*21*).

Circular Dichroism. In Figure 3, the 4 K CD and OD spectra are shown. The positions of the positive and negative bands are indicated. In the CD spectrum of the peridinin absorption region, peaks appear at 462, 510, 516, 537, and 545 nm. The bands at 407, 427, and 438 nm are most likely due to Chl *a*. Very similar peaks in the CD spectrum were reported in ref *6*. Note that the band at 438 nm, most likely due to the Chl *a* Soret band, is more pronounced here than in the spectrum reported in ref *6*.

In the 575−700 nm region, maxima at 585 and 625 nm and minima at 603, 615, and 666 nm are visible. The CD signal of the Chl *a* Q_y band is shifted 1 nm to the red (666 nm) with respect to the OD spectrum (665 nm) and is significantly narrower than the OD band. This was not reported for PCP of *A. carterae* before (*4*, *22*); however, for

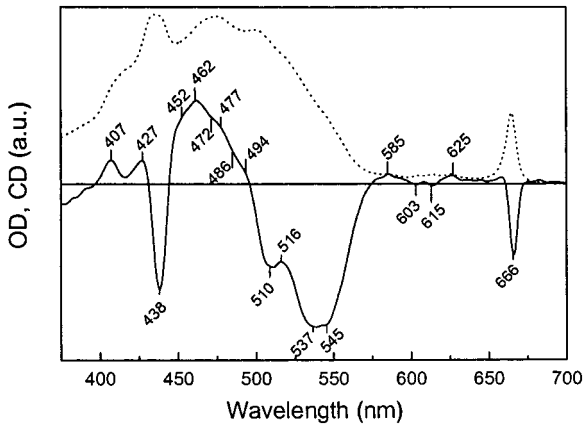

FIGURE 3: OD (dotted) and CD (solid) spectra of PCP measured at 4 K.

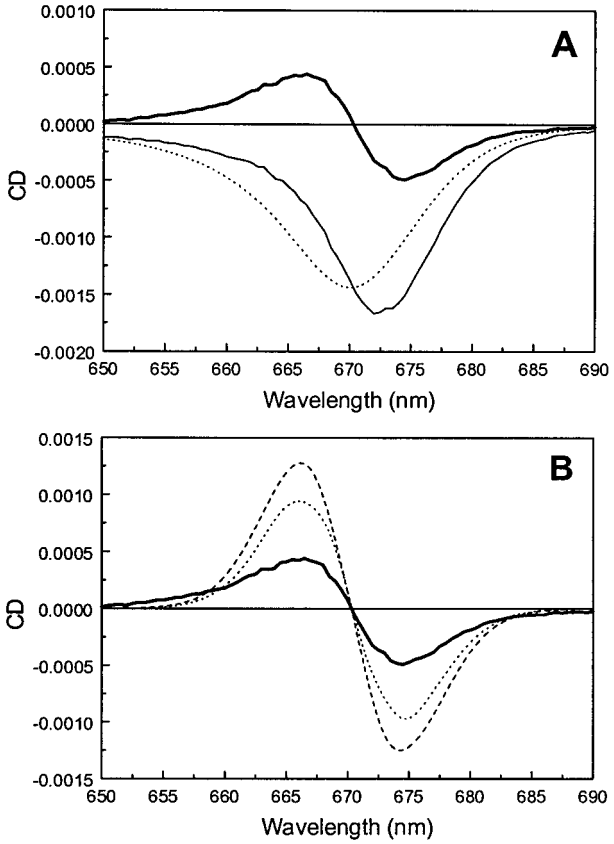

FIGURE 4: (A) CD spectrum (OD_{670} = 1) measured at RT (solid) in the 650−690 nm region. Also shown is the OD spectrum at RT (dotted), which is reversed in sign. The integrated area of the CD and OD spectra are normalized. The bold solid spectrum shows the difference spectrum (CD minus OD), which is the estimated conservative component of the CD spectrum (see text). (B) Smoothed simulated CD spectra for monomers (dashed) and for trimers (dotted). The bold solid spectrum shows the estimated conservative CD (of panel A).

PCP from *Alexandrum cohorticula* containing 12 peridinins and two Chls *a*, a red shift and a narrowing of the Chl *a* CD band was found as well (*23*). Figure 4A shows the CD spectrum (solid) in the 650−690 nm region measured at RT and the inverse OD spectrum (dotted) normalized to equal area with respect to the CD spectrum. Clearly, the CD and the OD spectrum do not have the same shape. This suggests that the CD spectrum is the sum of a conservative and nonconservative spectral component. Because the area of the

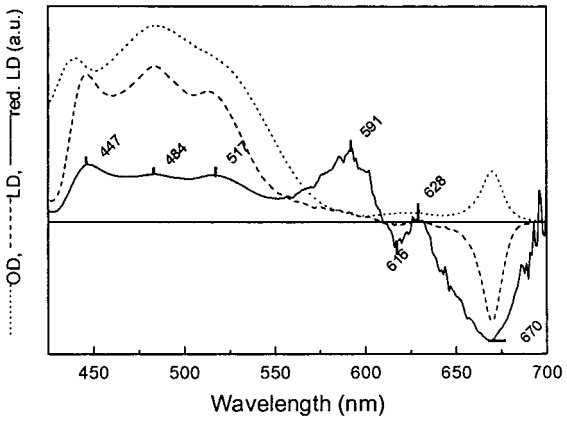

FIGURE 5: Room temperature LD (dashed), OD (dotted), and reduced LD (solid) spectra. The amplitude of the LD signal at 670 nm is $LD_{670} = \sim 5 \times 10^{-3}$ ($OD_{670} = 1$).

conservative spectrum is zero by definition, it can be found by subtracting the normalized OD spectrum from the CD spectrum, where it is assumed that the nonconservative CD spectrum has the shape of the OD spectrum. The bold solid spectrum in Figure 4A reflects the "conservative CD", and it has an amplitude of 5×10^{-4} ($OD_{670} = 1$ in the peak of the absorption spectrum at 670 nm). The amplitude of the RT CD signal at 672 nm is 1.8×10^{-3} ($OD_{670} = 1$). The nonconservative CD (inverse OD in Figure 4A) has an amplitude of 1.4×10^{-3}. This is much larger than the CD of monomeric Chl *a* in ether or detergent, which is on the order of $\sim 2 \times 10^{-4}$ (*19*). In the Discussion section, the estimated conservative spectrum is compared to the CD that is calculated on the basis of the structure.

Linear Dichroism. The room temperature OD, LD, and LD_r spectra are shown in Figure 5. Note that the Chl *a* Q_y peak has shifted 2.5 nm to the red with respect to the position of the Q_y band in 85% (v/v) glycerol at RT, probably due to the lower glycerol content (66% v/v) of the gel. The LD spectrum shows peaks at 447(+), 484(+), 517(+), and 670-(−) nm. The solid line in Figure 5 shows the reduced LD spectrum. The peaks are indicated in the spectrum. The reduced LD is 2−3 times smaller in the carotenoid region as compared to the Chl *a* Q_y region, and the signs are opposite. The positive features at 591 and 628 nm were reported before at similar wavelengths for the absorption spectrum of isolated Chl *a* and were assigned to the Q_x bands of Chl *a* (*19*, *20*).

In Figure 6A, the inverse LD (solid) and OD (dashed) spectra at 77 K of the Q_y region are plotted. The LD and OD spectra are normalized to 1 in the peaks. The peak of the LD spectrum is shifted 0.5 nm to shorter wavelengths with respect to that of the OD spectrum. In the Discussion section, this band shift will be interpreted in terms of the spectral positions of the absorption bands of the individual Chls *a*.

Fluorescence Anisotropy. The fluorescence anisotropy spectrum as a function of the excitation wavelength at room temperature is shown in Figure 7 (filled circles). To prevent depolarization of the fluorescence due to rotation of the whole molecule, PCP was dissolved in a (uncompressed) gelatin gel. The dashed spectrum shows the OD spectrum of PCP in the gel. The anisotropy at room temperature has a value of ~0.1 and is almost independent of the excitation

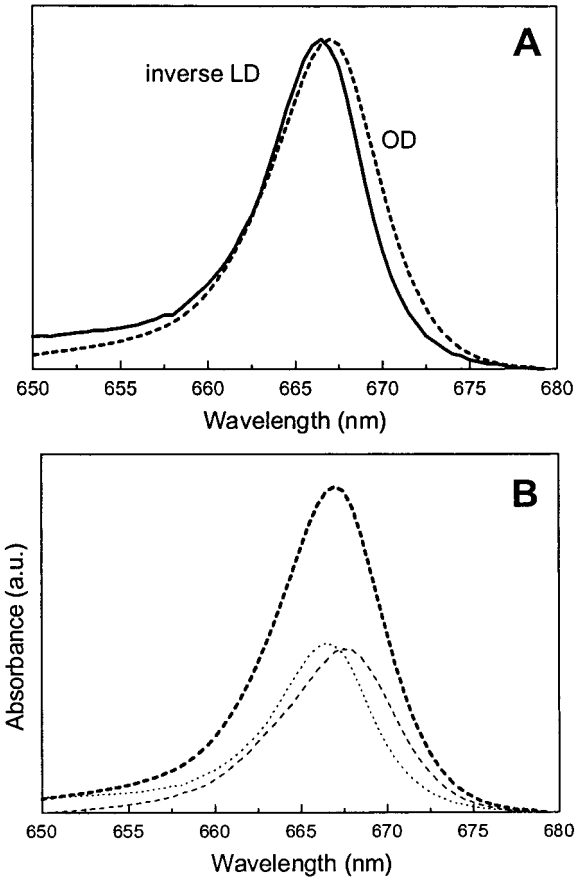

FIGURE 6: (A) LD (bold solid) and OD (bold dashed) spectra measured at 77 K. The LD spectrum is reversed. The spectra are normalized in the peaks. (B) Decomposition of the OD spectrum (bold dashed). The estimated absorption spectra of the individual Chls *a* are shown (dotted, dashed). The maxima are separated by ~1 nm (see text for details).

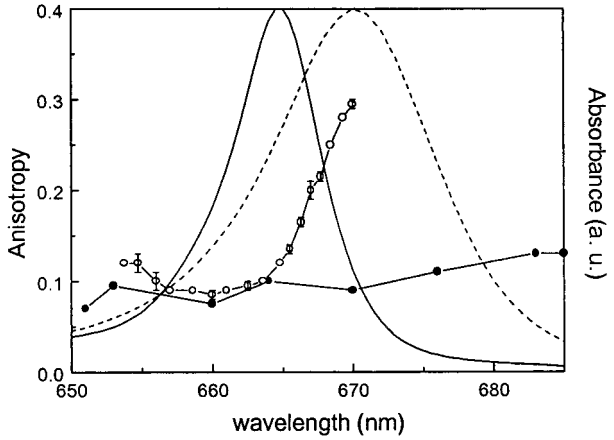

FIGURE 7: Fluorescence anisotropy spectrum of PCP at 4 K (open circles). The error bars indicate the upper and lower value of the anisotropy calculated from two sequential measurements at the same laser excitation wavelength. Also shown is the RT fluorescence anisotropy spectrum of PCP (filled circles). The RT anisotropy was measured in gelatin to immobilize the complexes. In addition, the OD spectra of PCP at 4 K (solid) and RT (dashed) are shown.

wavelength (slight increase at longer wavelengths is partly due to some scattering). Also shown in Figure 7 is the fluorescence anisotropy spectrum measured at 4 K (open circles) and the 4 K OD spectrum (solid). The anisotropy both at RT and at 4 K was independent of the detection wavelength. At 4 K, the anisotropy ranges from 0.08 at 660

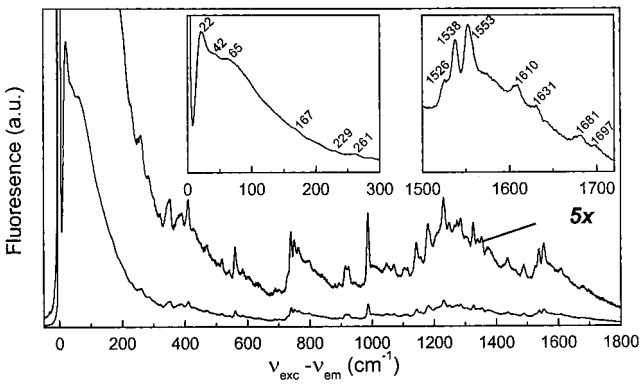

FIGURE 8: FLN spectrum of PCP measured at 4 K, where $\nu_{exc} - \nu_{em}$ is given in wavenumbers (cm^{-1}). Excitation was at 671 nm. Left inset shows an enlargement of the PW, and the right inset shows the vibrational fine structure in the 1500−1720 cm^{-1} region. The latter spectrum is the average of eight spectra excited at 668−671 nm.

nm to a value of 0.3 at 670 nm, which is close to the value of ∼0.35 that is expected in the absence of energy transfer. Generally, the theoretical maximum value of 0.4 that is reached when transition dipole moments for absorption and emission are parallel is not observed experimentally. Polarized fluorescence excitation spectra were reported in refs *3* and *4*, but the number of points in the Q_y region is too small for a detailed comparison.

Fluorescence Line Narrowing Spectroscopy. Figure 8 shows the FLN spectrum of PCP at 4 K after excitation in the red edge of the OD spectrum at 671 nm. Along the *x* axis the excitation frequency (ν_{exc}) minus the emission frequency (ν_{em}) is represented in wavenumbers. The upper spectrum is multiplied by 5. The FLN spectra were recorded at an OD of 0.4 in the Q_y maximum at 665 nm. At 671 nm, the OD is below 0.1 (see Figure 1) so that self-absorption, which could affect the shape of the emission spectrum, is very much reduced. The FLN spectrum consists of three parts: a sharp zero phonon line (ZPL) superimposed by scattered laser light, a relatively broad phonon wing (PW) on the red side of the ZPL, and sharp vibronic bands on top of the PW. The ZPL is due to the pure electronic transition. The PW is due to the coupling of the electronic transition to the intermolecular vibrations of the protein (electron−phonon bath). The vibronic coupling, that is, coupling to the intramolecular vibrations of the pigment, leads to a series of vibronic bands.

The left inset in Figure 8 shows a magnification of the PW. It shows considerable structure and has a pronounced main peak at 22 cm^{-1}, a shoulder at 42 cm^{-1}, and a broad feature at ∼65 cm^{-1}. For the emitting chlorophyll in the light-harvesting complex II of green plants (LHCII) (*8*) and in the Cytb_6f complex (*21*), just a main band at ∼20 cm^{-1} is observed, whereas in the case of the photosystem II reaction center complex (PSII RC) (*24*), a similar structure as for PCP was observed, with bands located at 19, 37, and 80 cm^{-1}. It is not known whether these extra bands have to be attributed to other modes or to a progression of the mode at ∼20 cm^{-1}. If in case of PCP the band at 65 cm^{-1} would be a separate mode originating from the coupling to other pigments and not due to the protein phonon bath, the only candidates for such a coupling would be the peridinins, since the coupling between the Chls is very weak (see Discussion).

The magnification of the 1500−1720 cm^{-1} region shown in the second inset of Figure 8 is an average of eight spectra excited at four different wavelengths (668−771 nm). The sharp lines are due to vibronic bands. The frequencies of these lines are independent of the excitation wavelength. In the 1500−1700 cm^{-1} region, the frequencies of the 13^1 C═O stretch mode of Chl *a* (1650−1700 cm^{-1}) and the C═C stretch modes of the chlorin ring are located (*25*, *26*). Bands visible at 1697 and 1681 cm^{-1} can be assigned to the 13^1 C═O stretch mode. The band at 1697 cm^{-1} reflects a non-H-bridged 13^1 C═O group. The band at 1681 cm^{-1} indicates a very weakly bound or unbound 13^1 C═O group. The fact that two different frequencies are observed suggests that either there are two different emitting Chls *a* or that the emitting Chl *a* can have two different environments. When the two Chls *a* have inhomogeneously broadened absorption bands that are only slightly shifted (see Discussion) with respect to each other, the red-most pigment in a complex can be either Chl a_1 or Chl a_2 (see Figure 10), and therefore the fluorescence most probably originates from both pigments. The fact that we do not find (strong) H bridges is in agreement with the structure (*2*).

The frequencies of the C═C stretch modes are located at 1526, 1553, and 1610 cm^{-1}. These frequencies indicate that the chlorins are five-coordinated. The frequencies of these modes would be 10 cm^{-1} lower when the chlorin would have been six-coordinated (25, 26). From the structure, it is known that the fifth coordination site is formed by a water molecule (*2*).

T-S Spectroscopy. Transient absorption traces induced by selective excitation of Chl *a* at 590 nm, were recorded at detection wavelengths ranging from 400 to 700 nm, both at room temperature and at 77 K. They reflect the decay of triplet states formed in the complex. These traces were fitted using a global analysis routine (*10*). At RT, the data could be fitted with one lifetime component of 10 μs, which is characteristic for carotenoid triplets. No lifetime component of hundreds of microseconds or a few milliseconds, typical for Chl triplets, was found. Apparently, chlorophyll triplets are transferred to peridinin with an efficiency of 100%, in agreement with the findings in ref *5*. The decay associated difference spectra (DADS) are shown in Figure 9A (squares). In the peridinin absorption region, a broad bleaching is visible at 450 nm, and positive features due to absorption by the triplet states are located at 555 and 593 nm. In the Q_y region that is shown in Figure 9B (squares), at ∼668 nm clearly a bleaching is visible, reflecting Chl *a* absorption changes due to the presence of a triplet on a neighboring peridinin. A similar signal in the 10 μs T-S component has been observed for LHCII (*27*).

At 77 K, besides a 13 μs component, a spectrally different second component with a lifetime of 40 μs was needed for an adequate fit of the data. The spectra are shown in Figure 9A. The 13 μs 77 K component (triangles) is spectrally very similar to the 10 μs RT component (squares). However, in the 77 K spectrum (see magnification in Figure 9C) shoulders and peaks at 515, 554, 567, and 589 nm are better resolved. The 40 μs component (circles) has, when compared to the 13 μs component, a more pronounced peak at 515 nm and a stronger bleaching at 505 and 534 nm (see Figure 9C). In the Discussion section, the T-S peaks will be discussed in more detail. The two DADS are also slightly different in

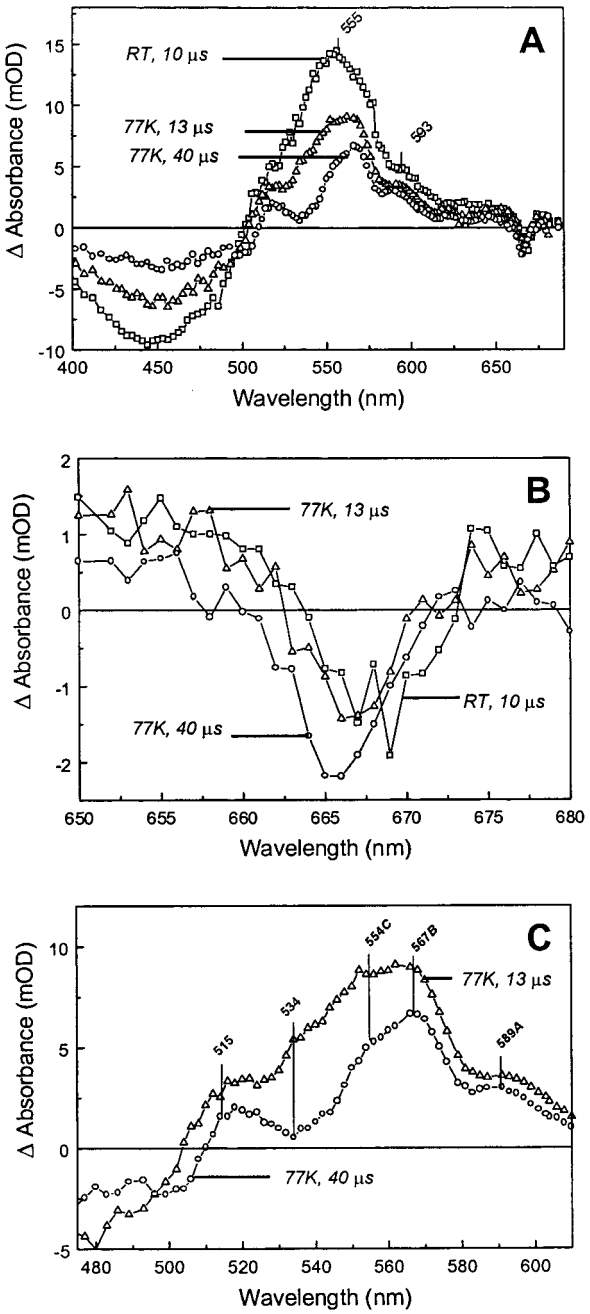

FIGURE 9: T-S DADS at 77 K and RT. (A) DADS of the 10 μs component measured at RT (open squares) ($OD_{670} = 0.15$). Also shown are the DADS of the 13 (open triangles) and 40 μs component (open circles) measured at 77 K ($OD_{665} = 0.23$) (B) Enlargement of panel A in the Q_y region. (C) Enlargement of the 77 K spectra shown in panel A in the peridinin region.

the Q_y region; however, due to the low signal-to-noise, this might not be significant (see Figure 9B). The fact that two components with different lifetimes are present is not easy to explain. For a fit of T-S data of LHCII at 4 K, two lifetimes of 8 and 40 μs were needed (*27*); however, the corresponding T-S spectra were identical. The 8 and 40 μs components were attributed to decays of different triplet sublevels (*27*). If that would be the explanation in the case of PCP, it is remarkable that (i) the effect would already be visible at 77 K and (ii) it apparently just happens only in one or a few peridinins. Another explanation for the 40 μs component could be that at 77 K, besides triplets with a lifetime of 13 μs, triplets also are formed on one or more peridinins that have a longer triplet lifetime. An extensive examination of the temperature dependence of the T-S spectra of PCP might shine more light on this issue.

DISCUSSION

Monomers and Trimers. Using the crystal structure of PCP, in principle, CD and LD spectra and the value of the residual anisotropy can be calculated. However, a comparison of these calculations with the experimental data is hampered by the fact that the preparation does not contain only trimeric complexes. This can be concluded from the fact that the measured residual anisotropy at RT has a value of ~0.1, which is higher than the value of the residual anisotropy calculated on the basis of the trimeric structure, which is 0.05 (*17*). For monomeric PCP, an expected value of 0.15 was calculated (*17*). Apparently, the preparation consists of a mixture of monomers and trimers. Using ultracentrifugation techniques, it was shown that the relative amounts of monomers and trimers depend on the PCP concentration of the preparation (Hofmann et al., unpublished results). Since the biochemical separation of monomers and trimers cannot be done without affecting the monomer/trimer equilibrium, we have not been able to determine the amounts of monomers and trimers at a certain concentration. An additional problem is that it is not known whether this equilibrium is affected by the presence of gelatin or glycerol and how fast a new equilibrium is reached after dilution.

Chl a in PCP. From LD, OD, and FLN experiments, a wealth of information can be obtained about the local environment of the Chls *a* in PCP. On the basis of a comparison of the LD measurements with the LD that is calculated on the basis of the crystal structure, we will discuss whether the Chls *a* in PCP are isoenergetic. Using the OD spectra measured at different temperatures together with the PW, we will determine the width of the inhomogeneous distribution function (IDF). In addition, the Huang−Rhys factor, which expresses the strength of the electron−phonon coupling, will be calculated.

Since we do not know the relative amounts of monomers and trimers, we will calculate the reduced LD on the basis of the crystal structure for both monomeric and trimeric PCP. The orientation behavior in a gel is different for monomers (more or less with a rodlike shape) and trimers (disklike shape). For trimers, the angles ζ (see eq 1) are defined with respect to the axis oriented perpendicular to the plane of the trimer (*11*). In case of monomers, the choice of the molecular axis is more difficult since the "length" of the monomeric particle is only about twice the "width". The axis through the magnesium atoms of the two chlorophyll molecules seems to be a reasonable choice. The Q_x and Q_y transition dipole moments of the Chl *a* molecules are assumed to be oriented along the NA−NC and NB−ND axis, respectively (notation as in ref *2*). In ref *17*, it was concluded that the orientation of the Q_y transition dipole moment of Chl *a* in PCP can very well be approximated by the orientation of the NB−ND axis. The transition dipole moment of peridinin in principle lies parallel to the long axis of the molecule; however, some of the peridinins are slightly bent. We have assumed the transition dipole moment to be oriented along C_6-C_{24} (numbering as in ref *2*). Since the amplitude of the orientation factor (ϕ_n) is not known, only the shape of the spectrum and the relative sizes of the peaks can be calculated.

Table 1: Angles and LD with Respect to Monomer and Trimer Symmetry Axis[a]

	trimer symmetry axes			monomer Mg−Mg symmetry axes		
transition dipole moment	angle	reduced LD	avg	angle	reduced LD	avg
Chl a_1 Q_x	59	0.10	0.30	62	−0.17	−0.16
Chl a_2 Q_x	88	0.50		61	−0.15	
Chl a_1 Q_y	58	0.08	−0.33	87	−0.50	−0.50
Chl a_2 Q_y	25	−0.73		87	−0.50	
Per 11 C_6−C_{24}	63	0.19	0.06	48	0.17	−0.13
Per 12 C_6−C_{24}	54	−0.02		74	−0.39	
Per 13 C_6−C_{24}	65	0.23		44	0.28	
Per 14 C_6−C_{24}	49	−0.15		87	−0.50	
Per 21 C_6−C_{24}	65	0.23		48	0.17	
Per 22 C_6−C_{24}	89	0.50		78	−0.44	
Per 23 C_6−C_{24}	70	0.32		47	0.20	
Per 24 C_6−C_{24}	21	−0.81		87	−0.50	

[a] Note that LD values for trimers are multiplied by −1 because disklike particles have a negative orientation factor. The Chls *a* and peridinins (Per) are numbered according to ref *2*.

In Table 1, the calculated values of ζ and the LD_r for peridinin and Chl *a* (Q_y and Q_x transitions) in monomeric and trimeric PCP are given. The experimentally determined LD spectrum is the sum of the contributions of the individual pigments in each absorption region. Therefore, in Table 1, the average values of LD_r in the peridinin Q_x and Q_y regions also are given. Note that ϕ_n is negative for trimers and positive for monomers. In case of monomers, the average value of LD_r is negative in the Q_x and Q_y and peridinin absorption region, whereas for trimers, it is positive in both the peridinin and the Q_x region and negative in the Q_y region. The measured spectrum (see Figure 5) is clearly in disagreement with the calculated values for monomers and resembles the calculated trimer spectrum. Since from anisotropy experiments it was concluded that the preparation consists of a mixture of monomers and trimers, this might imply that the orientation of monomers in the gel is worse than that of trimers. The calculations predict that the LD_r amplitudes of the two Chl *a* Q_y transitions in trimers have different values (0.08 and −0.73), while in monomers they are the same (−0.50) (see Table 1). The equal amplitudes in the monomer case cannot explain the shift of the peak of the LD spectrum with respect to that of the OD spectrum as was detected for the 77 K LD and OD spectra (see Figure 6). Only in case of trimers the difference in amplitude can show up in the spectra, provided that the Chl *a* molecules are absorbing at different wavelengths.

Assuming that the complex we observe in LD is organized in trimers, it is possible to estimate the peak positions of the Q_y transitions of the two Chls using the OD and LD spectra measured at 77 K. The OD and LD spectra are normalized to equal area in the 650−680 nm region. The OD spectrum is assumed to consist of the absorption bands of the individual Chls (OD_a and OD_b) with equally weighted amplitudes: $OD = OD_a + OD_b$. The LD spectrum can be described as a linear combination of OD_a and OD_b according to $LD = c_aOD_a + c_bOD_b$. Because the areas of the OD and LD spectrum are normalized, we have $c_a + c_b = 2$. The ratio $x = c_a/c_b$ is given by $c_a/c_b = (\langle 1/2(3\cos^2 \zeta_a - 1)\rangle \phi_n)/(\langle 1/2(3\cos^2 \zeta_b - 1)\rangle \phi_n)$. The preceding four expressions can now be combined into one for OD_b:

$$OD_b = \frac{x}{x-1}OD + \frac{1}{2}\frac{1+x}{1-x}LD \qquad (6)$$

from which $OD_a = OD - OD_b$ is easily obtained. For Chl a_1 and Chl a_2, x has a value of −9 (see Table 1). In Figure 6B, the decomposition (dotted and dashed) of the OD spectrum (bold dashed) is shown. We find that the OD_a and OD_b spectra are shifted by ∼1 nm with respect to each other, much less than the fwhm of the Q_y band. Chl a_1 (see Figure 10) has the red-most OD spectrum. As discussed, we assumed that the LD spectrum is entirely due to trimeric PCP. If the LD spectrum is the sum of the LD spectra of monomeric and trimeric PCP, the interpretation of the shift is more complicated. Because the LD signal is dominated by the trimers, the possible contribution of the monomers will only slightly change the mutual shift.

To obtain information about the electron−phonon coupling strength, which is expressed in the Huang−Rhys factor (*S*), and about the inhomogeneous distribution function (IDF), we have simulated the temperature dependence of the absorption spectra in the Chl *a* Q_y region. The algorithm that is used has been described extensively elsewhere (*28*) and is based on linear, harmonic Franck−Condon electron−phonon coupling and assumes a temperature-independent inhomogeneous distribution function (IDF). The PW obtained from site-selected excitation at 675 nm is assumed to resemble the single-site emission spectrum, and it provided the input for the simulation. Since *S* is not known, different values of *S* were used to simulate the temperature-dependent homogeneous spectra, which were then convoluted with a Gaussian IDF. Simulated and measured spectra were compared via the second moment of the Q_y absorption band, which forms a measure for the bandwidth. The second moment was calculated over the interval where the absorption was >30% of the maximum of the Q_y absorption to minimize uncertainties due to possible (small) baseline offsets. Figure 11 shows the temperature dependence of the second moment of the simulated and measured spectra. The best agreement between simulation and experiment is achieved when $S = 1.0$, and the width (fwhm) of the IDF is 160 cm^{-1}. The broadening of the absorption spectrum could well be simulated up to 250 K. Above this temperature, simulation and experiment start to deviate, possibly due to contributions of nonlinear electron−phonon coupling and/or a change in the IDF.

The value of 1.0 that is found for the Huang−Rhys factor in case of PCP is moderately large as compared to the values found for other pigment−protein complexes. For LHCII and Cytb_6f, values of 0.6 ± 0.1 and 0.6−0.9, respectively, were found (*8*, *21*). The value that is found for the Huang−Rhys factor of the PSII RC is 1.6 ± 0.3 (*24*). The IDF of Chl *a* in PCP (160 cm^{-1}) is larger than that of Chl *a* in LHCII (120 ± 15 cm^{-1}) and smaller than that of Chl *a* in Cytb_6f (210 ± 10 cm^{-1}).

In Figure 12A, the measured and simulated spectra (corresponding to *S* and IDF values of 1.0 and 160 cm^{-1}, respectively) are shown. All amplitudes of the measured spectra have been scaled with the same factor for comparison with the simulated spectra. For each temperature, the measured spectrum has been shifted until the maximum coincided with that of the simulated spectrum. Note that a shift of the ZPL is not included in the model, so only the

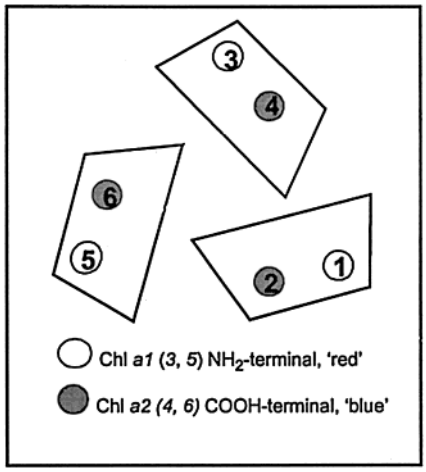

FIGURE 10: Simplified representation of Chls *a* in trimeric PCP.

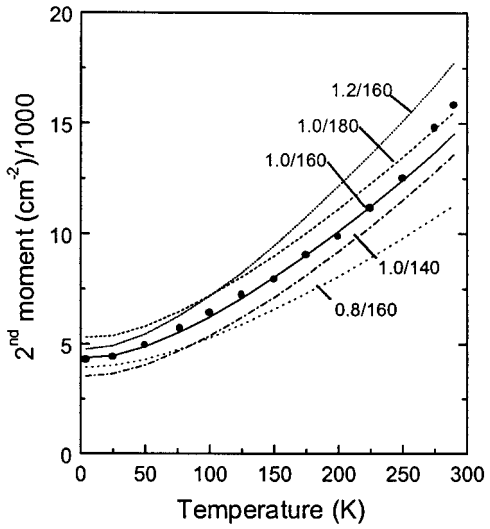

FIGURE 11: Comparison between the experimental (filled circles) and the simulated temperature dependence of the second moment of the Chl *a* Q_y band in PCP (see text). The values for *S* and the width (in cm^{-1}) of the inhomogeneous distribution function were as indicated.

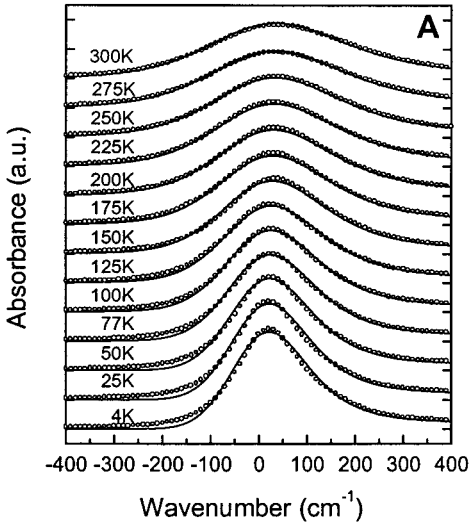

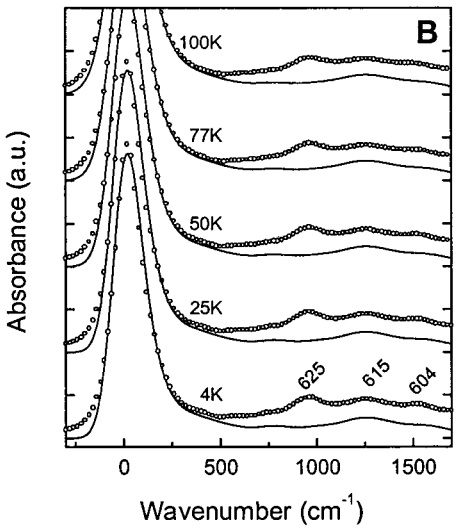

FIGURE 12: (A) Comparison between the experimental absorption spectra and the simulated spectra at temperatures ranging from RT to 4 K for $S = 1$ and a width of the IDF of 160 cm^{-1}. (B) As in panel A, but for the temperatures 4, 25, 50, 77, and 100 K including the absorption region to the blue of the Q_y band. Also indicated are the wavelengths in nm.

shape of the band can be modeled. From 125 to 290 K, the simulated and measured spectra correspond reasonably well. Below ~125 K, the line shapes start to deviate. This might be because we did not take into account the possible small difference in site energies between the two Chls *a* in PCP and thus used only one Gaussian IDF. A more sophisticated line shape of the IDF might lead to some improvement of the simulation, but this is beyond the goal of this paper. Figure 12B shows the Q_x and Q_y regions of the simulated and measured spectra for 4, 25, 50, 77, and 100 K. Clearly, the simulated spectra show the bands at 615 and 604 nm, which are also present in the experimental spectrum. The band at 625 nm that is visible in the measured spectrum cannot be distinguished in the simulated spectrum. This suggests that the bands at 615 and ~604 nm in the absorption spectrum should (at least partially) be attributed to vibronic bands coupled to the (electronic) Q_y transition. We conclude that the band at 625 nm is due to the electronic Q_x transition. The orientation of the transition dipole moment of a vibronic band coupled to the Q_y transition will approximately be the same as that of the pure electronic transition. As a consequence, the signs of the LD and CD signals of these bands and the Q_y band, in the absence of exciton coupling, are expected to be the same. In the CD spectrum (Figure 3) indeed the 603, 615, and 666 nm bands have the same sign, whereas the band at 625 nm has an opposite sign. The LD spectrum (Figure 5) clearly shows a maximum at 628 nm and a minimum at 616 nm. At 604 nm, no band can be distinguished. Apparently, the CD and LD spectra support the notion that the bands at 605 and 614 nm are due to vibrations coupled to the electronic Q_y transition.

Peridinin in PCP. Even at 4 K, a limited amount of structure is visible in the absorption spectrum of PCP in the peridinin absorption region due to the many overlapping absorption bands (Figure 1A,B). It is therefore very difficult to identify the individual peridinins in the PCP absorption spectrum. Nevertheless, by using a combination of the spectral information from OD, LD, CD, and T-S measurements and the absorption spectrum of peridinin in a solvent, we will tentatively assign some of the bands in the PCP absorption spectrum to individual peridinins. Since it was reported by Carbonera et al. (*29*) that the PCP absorption spectrum is not strongly affected by exciton coupling, we

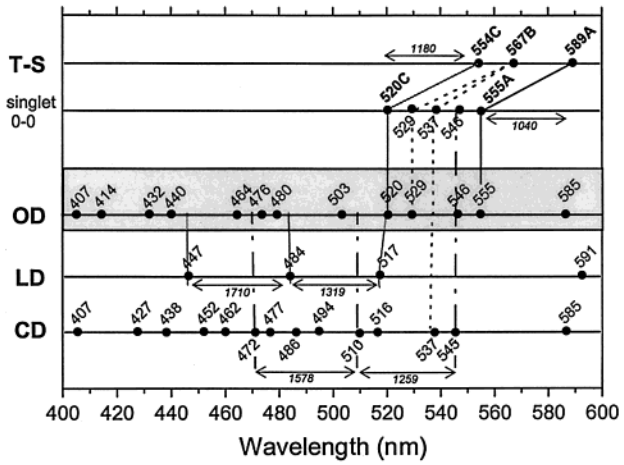

FIGURE 13: Summary of the spectroscopic features in PCP as detected in T-S, OD (second derivative Figure 1B), LD, and CD spectra. The energy differences between some spectral features are indicated with arrows. The value of the energy difference (in cm^{-1}) is italicized (see text for details).

will not take that coupling into account in the following analysis. Figure 13 gives an overview of the spectral features, repesented by bullets, that are observed in T-S, OD, LD, and CD spectra.

The absorption spectra of peridinin in both ethanol (77 K) (*4*) and methanol (RT) (*30*) show a peak at 475 nm and shoulders at ~445 and 505−509 nm, whereas in *n*-hexane, the spectrum shows a shoulder at ~426 nm and peaks at 456 and 486 nm (*5*). The bands have to be attributed to the electronic S_0-S_2 transition, and the red-most band in each solvent corresponds to the vibronic 0−0 transition. In these solvents, the spacing between the vibronic bands of peridinin is about the same, ~1410 cm^{-1} on average. It is therefore likely that also in PCP the spectrum of an individual peridinin is characterized by this typical band pattern, although the relative intensities of the bands can vary. However, it should be noted that the spacing between the vibronic bands of peridinin in PCP might be affected by exciton interactions.

In the 77 K T-S spectra shown in Figure 9C, positive peaks are located at 589, 567, and 554 nm. In refs *31* and *32*, it was shown that a carotenoid triplet spectrum can be represented by the ground-state absorption spectrum shifted to longer wavelength. Since the 554 nm band cannot be a vibronic band of the 589 nm transition because the energy difference is too small, 1073 cm^{-1} instead of 1410 cm^{-1} (see above), the three T−S maxima most likely correspond to individual peridinins. It should be emphasized that the shorter the wavelength the more the maxima and minima overlap and the more uncertain the peak positions are.

In the absorption spectrum, the longest wavelength peak is located at 555 nm (see Figures 1B and 13). Above that wavelength, no clear features are observed, and the band at 585 nm was assigned to Chl *a*. The next peridinin absorption band is located at 546 nm (see Figures 1B and 13). In the CD spectrum, a negative band at 545 nm is also visible, and negative bands are observed at 510 and 472 nm, possibly due to the corresponding vibronic bands (see Figure 13). The relatively small absorption band at 529 nm cannot directly be related to any band observed with another technique. The absorption band at 520 nm might be a vibronic band of the 0−0 transition at 555 nm. However, it seems more likely that it corresponds to the 517 nm LD band. The LD band pattern suggests that the LD is mainly determined by a peridinin that has its absorption bands at 517, 484, and 447 nm (see Figure 13) and not near 555 nm. We thus find evidence for at least three different peridinins on the basis of OD, LD, and CD.

The individual peridinins distinguished in the T-S spectrum now have to be linked to those discussed in the previous paragraph. The longest wavelength singlet peak at 555 nm most likely corresponds to the longest wavelength T-S peak at 589 nm. The energy difference (ΔE_A) between the T-S peak at 589 nm and the OD peak at 555 nm is 1040 cm^{-1} (see Figure 13). The singlet peak at 520 nm is most probably linked to the 554 nm T-S peak. The energy difference is 1180 cm^{-1}(ΔE_C). If we suppose for the 567 nm T-S band an energy difference ΔE_A, we would expect a singlet band at 535 nm. At 537 nm, a CD band is visible. On the other hand, if an energy difference of ΔE_C is supposed, we would expect a singlet band at 531 nm. This might correspond to the 529 nm absorption band. In conclusion, we cannot unambiguously correlate the 567 nm T-S band with an absorption band.

We have found evidence that at least four peridinins that have their electronic transitions at 520, 529 or 537, 546, and 555 nm determine the T-S, OD, LD, and CD spectra of PCP. On the basis of the crystal structure of PCP, one would expect that at least the four peridinins in one cluster do not have the same absorption spectra since each of these peridinins experiences a slightly different local environment. Nevertheless, it should be emphasized that our assignment only gives a lower limit to the number of contributing peridinins. According to the simulation of the CD and OD spectra by Carbonera et al., the electronic transitions, in the absence of exciton coupling, are located at 485, 518, 534, and 543 nm at 20 K (*29*). The authors state that the absorption spectrum is not strongly affected by exciton coupling (*29*), so that these wavelengths can be compared to the ones we have determined using a different approach. In both cases, the bands are distributed over a large wavelength region. Three of the four bands are located at very similar wavelengths. We do not find evidence for a band at 485 nm, but due to the many overlapping bands we cannot exclude a band at that position.

Chl a−Chl a Interactions. As was stated in the introduction, the peridinin to Chl *a* excitation energy transfer in PCP is very fast (*5*). Since PCP functions as a light-harvesting complex, the energy has to be transported finally to the PSII complex. One might therefore expect that also Chl *a* to Chl *a* excitation energy transfer takes place within PCP. The anisotropy measurements presented in this paper confirm the occurrence of Chl *a* to Chl *a* transfer processes. When no transfer between pigments occurs, the Stokes shift, which is the difference in position between the absorption and the fluorescence maxima, equals $2S\omega_m$, where S is the Huang−Rhys factor, and ω_m is the mean phonon frequency (see for example, ref *33*). In this case, that relation does not hold since the Stokes shift is 77 cm^{-1}, and $2S\omega_m = 44$ cm^{-1}, thus confirming that Chl *a* to Chl *a* energy transfer takes place. Direct measurement of the Chl *a* to Chl *a* transfer in PCP using time-resolved fluorescence anisotropy measurements yielded two depolarization times that were assigned to equilibration within the monomer (~7 ps) and equilibration within the trimer (350 ps) (*17*). A prerequisite for

excitation energy transfer between pigments is that the interacting pigments should at least be weakly coupled. In the following paragraphs, we will determine the coupling and simulate the CD spectrum of PCP in the Chl *a* region.

To investigate whether the conservative part of the CD in the Q_y region is entirely due to exciton interaction between the Chls *a* within a monomer or whether also interactions in the trimer have to be included, we have simulated the CD of PCP. The exciton interaction energy was calculated from the structure (with the Q_y transition dipole moment oriented parallel to the NB−ND axis), both for PCP trimers and monomers (see Materials and Methods). For the effective dipole strengths, we used a value of 17 D^2. The Gaussian distribution function had a fwhm of 280 cm^{-1}, which was necessary to correctly describe the bandwidth of the OD spectrum at room temperature. The width here is larger than the width of the IDF in the simulations of the absorption spectra at different temperatures (160 cm^{-1}) because it now accounts for both homogeneous and inhomogeneous broadening. As was already stated in Materials and Methods, it is not necessary to distinguish between both types of broadening for the CD calculations. The site energies of the two Chls *a* within one monomer were assumed to be equal, but shifting the site energies apart led to virtually identical spectra as long as the splitting was small as compared to the total bandwidth. For instance, a splitting of 100 cm^{-1}, which is already much larger than could be concluded from a comparison of the absorption and LD spectra, still gave rise to almost indistinguishable spectra. The exciton interaction energy within a monomer was calculated to be ~ -7 cm^{-1}.

Figure 4B shows the experimental and simulated CD spectra obtained with the previously discussed parameters. The shapes of the simulated (dotted, dashed) and measured spectra (bold solid) are very similar. The simulated CD spectrum of the trimer (dotted) is smaller than that of the monomer (dashed); however, both spectra are larger than the experimentally determined CD spectrum. Apparently, other interactions also contribute to the CD. It was already mentioned in the Results section that the estimated nonconservative CD in the Q_y region is significantly larger than that of "free" Chl *a*, probably due to peridinin−Chl *a* interactions. If these interactions are not identical for both Chls *a*, then this will also lead to a contribution to the estimated conservative spectrum.

Peridinin−Chl a Interactions. Each peridinin in PCP is in van der Waals contact with Chl *a*. Therefore, strong interactions between peridinin and Chl *a* are to be expected. Exciton interactions between Chl *a* and peridinin, in principle, could involve any peridinin or Chl *a* transition. However, because the OD and CD spectra in the peridinin and Soret absorption region are difficult to interpret, we cannot determine whether the Chl *a* Soret transition contributes to the coupling between peridinin and Chl *a*. It was argued previously that the CD in the Q_y region indicates the presence of interactions between Chl *a* and peridinin.

The signal that is visible in the Q_y region in the T-S spectrum (Figure 9A,B) has a lifetime that corresponds to that of peridinin triplets, indicating that the presence of a triplet on peridinin influences the absorption of Chl *a*. Therefore, the T-S data also demonstrate the close interaction between Chl *a* and peridinin molecules.

The Chl *a* fluorescence PW (Figure 8) shows bands at 42 and 65 cm^{-1}. These bands are also visible in the calculated distribution of phonon and vibrational modes (*28*) (not shown), which implies that they originate from different modes rather than that they are due to overtones of the 22 cm^{-1} mode. These modes could be due to the protein, but it is also possible that they result from interactions between Chl *a* and peridinin.

CONCLUSIONS

The conclusions from the study presented in this paper can be summarized as follows:

(1) Chl *a* in PCP is five-coordinated, and the 13^1-keto carbonyl group is not or is very weakly H-bridged (FLN). These observations are in agreement with the structure (*2*).

(2) The Huang−Rhys factor has a value of 1, which is larger than that of LHCII (*8*) and Cytb_6f (*21*) and smaller than that of the PSII RC complex (*24*). The IDF has a fwhm of 160 cm^{-1}.

(3) Chl *a*−peridinin coupling is reflected by the following results: (i) the Chl *a* to peridinin triplet excitation energy transfer has an efficiency of 100%; (ii) the microsecond T-S spectra show a signal in the Q_y region indicating contact between Chl *a* and peridinin; (iii) the nonconservative CD in the Chl *a* region is much larger than the CD of monomeric Chl *a* in, for example, detergent; (*19*) and (iv) we speculate that the feature at 64 cm^{-1} in the PW reflects coupling between Chl *a* and peridinin.

(4) At room temperature, the Chls *a* in PCP are approximately isoenergetic.

(5) The two Chl *a* molecules in a PCP monomer are weakly coupled ($V \approx -7$ cm^{-1}), and the coupling between the Chls *a* within the trimer is even smaller. The CD spectrum that was simulated using these exciton interaction energies, is a factor of 2−2.5 larger than the experimentally determined spectrum. This is probably due to Chl *a*−peridinin interactions.

(6) Four different peridinins can be recognized in the T-S and OD spectra that are assigned to peridinins that have their red-most transitions at 520, 529−537, 546, and 555 nm.

(7) The intriguing observation that at 77 K an additional triplet lifetime component of 40 μs is present remains unexplained.

ACKNOWLEDGMENT

We thank Dr. Jan P. Dekker for useful comments.

REFERENCES

1. Van Grondelle, R., Dekker, J. P., Gillbro, T., and Sundström, V. (1994) *Biochim. Biophys. Acta 1187*, 1−65.
2. Hofmann, E., Wrench, P., Sharples, F. P., Hiller, R. G., Welte, W., and Diederichs, K. (1996) *Science 272*, 1788−1791.
3. Song, P.-S, Koka, P., and Prezelin, B. B. (1976) *Biochemistry 15*, 4442−4427.
4. Koka, P., and Song, P. (1977) *Biochim. Biophys. Acta 495*, 220−231.
5. Bautista, J. A., Atticks, K., Hiller, R. G., Sharples, F. P., Gosztola, D., Wasielewski, M., and Frank, H. A. (1999) *J. Phys. Chem. A 103*, 2267−2273.
6. Carbonera, C. G., Giacometti, G., and Segre, U. (1996) *J. Chem. Soc., Faraday Trans. 92*, 989−993.

7. Nussberger, S., Dekker, J. P., Kühlbrandt, W., van Bolhuis, B. M., van Grondelle, R., and van Amerongen, H. (1994) *Biochemistry 33*, 14775−14783.
8. Peterman, E. J. G., Pullerits, T., van Grondelle, R., and van Amerongen, H. (1997) *J. Phys. Chem. B 101*, 4448−4457.
9. Van Mourik, F., van der Oord, J. R., Visscher, K. J., Parkes-Loach, P. S., Loach, P. A., Visschers, R. W., and van Grondelle, R. (1991) *Biochim. Biophys. Acta 1059*, 111−119.
10. Van Stokkum, I. H. M., Scherer, T., Brouwer, A. M., and Verhoeven, J. W. (1994) *J. Phys. Chem. 98*, 852−866.
11. Van Amerongen, H., and Struve, W. S. (1995) *Methods Enzymol. 245*, 259−283.
12. Monshouwer, R., Abrahamsson, M., van Mourik, F., and van Grondelle, R. (1997) *J. Phys. Chem. B 101*, 7241−7248.
13. Pearlstein, R. M. (1991) in *Chlorophylls* (Scheer, H., Ed.) Chapter 4.11, CRC Press, Bota Raton, FL.
14. Alden, R. G., Johnson, E., Nagarajan, V., Parson, W. W., Law, C. J., and Cogdell, R. G. (1997) *J. Phys. Chem. B 101*, 4667−4680.
15. Jackson, J. D. (1975) *Classical Electrodynamics*, John Wiley & Sons, New York.
16. Pullerits, T., Chachisvilis, M., and Sundström, V. (1996) *J. Phys. Chem. 100*, 10787−10792.
17. Kleima, F. J., Hofmann, E., Gobets, B., van Stokkum, I. H. M., van Grondelle, R., Diederichs, K., and van Amerongen, H. (2000) *Biophys. J. 78*, 344−353.
18. Somsen, O. J. G., van Grondelle, R., and van Amerongen, H. (1996) *Biophys. J. 71*, 1934−1951.
19. Kwa, S. L. S., Völker, S., Tilly, N. T., van Grondelle, R., and Dekker, J. P. (1994) *Photochem. Photobiol. 59*, 219−228.
20. Van Zandvoort, M. A. M. J., Wrobel, D., Lettinga, P., van Ginkel, G., and Levine, Y. K. (1995) *Photochem. Photobiol. 62*, 299−308.
21. Peterman, E. J. G., Wenk, S.-O., Pullerits, T., Pålsson, L.-O., van Grondelle, R., Dekker, J. P., Rögner, M., and van Amerongen, H. (1998) *Biophys. J. 75*, 389−398.
22. Carbonera, D., Giacometti, G., and Agostini, G. (1995) *Spectrochim. Acta 51A*, 115−123.
23. Ogata, T., Kodama, M., Nomura, S., Kobayashi, M., Nozawa, T., Katoh, T., and Mimuro, M. (1994) *FEBS Lett. 365*, 367−371.
24. Peterman, E. J. G., van Amerongen, H., van Grondelle, R., and Dekker, J. P. (1998) *Proc. Natl. Acad. Sci. U.S.A. 95*, 6128−6133.
25. Fujiwara, M., and Tasumi, M. (1986) *J. Phys. Chem. 90*, 250−255.
26. Fujiwara, M., and Tasumi, M. (1986) *J. Phys. Chem. 90*, 5646−5650.
27. Peterman, E. J. G., Dukker, F. M., van Grondelle, R., and van Amerongen, H. (1995) *Biophys. J. 69*, 2670−2678.
28. Pullerits, T., Monshouwer, R., van Mourik, F., and van Grondelle, R. (1995) *Chem. Phys. 194*, 395−407.
29. Carbonera, D., Giacometti, G., Serge, U., Hofmann, E., and Hiller, R. G. (1999) *J. Phys. Chem. B. 103*, 6349−6356.
30. Akimoto, S., Takaichi, S., Ogata, T., Nishimura, Y., Yamazaki, I., and Mimuro, M. (1996) *Chem. Phys. Lett. 260*, 147−152.
31. Bensasson, R. V., Land, E. J., and Truscott, T. G. (1983) *Flash Photolysis and Pulse Radiolysis*, Pergamon Press, New York.
32. Aust, V., Angerhofer, A., Ullrich, J., von Schütz, J. U., Wolf, H. C., and Cogdell, R. J. (1991) *Chem. Phys. Lett. 181*, 213−221.
33. Reddy, N. R. S., van Amerongen, H., Kwa, S. L. S., van Grondelle, R., and Small, G. J. (1994) *J. Phys. Chem. 98*, 4729−4735.

BI992427S